IEEE Transactions on Nuclear Science, Vol. NS-30, No. 4, August 1983

HIGH POWER MICROWAVE GENERATION FROM ROTATING E-LAYERS IN MAGNETRON-TYPE CONDUCTING BOUNDARY SYSTEMS*

C. D. Striffler, W. W. Destler, R. Kulkarni, and R. L. Weiler

Electrical Engineering Department and
Laboratory for Plasma and Fusion Energy Studies
University of Maryland
College Park, Maryland 20742

Summary

Studies of the production of microwave and millimeter wave radiation at high harmonics of the relativistic electron cyclotron frequency by the interaction of a rotating E-layer with a multi-resonator magnetron boundary system have been conducted. The interaction of a 2 MeV, 1-2 kA, 5 ns cusp injected E layer of radius 6 cm with 12, 20, and 40 slot magnetron type waveguides are studied. Approximately 10% of the injected electron beam power is converted to microwaves at $12\ \omega_c$ (10 GHz), 2% at $20\ \omega_c$ (17 GHz), and 1% at $40\omega_c$ (34 GHz). We have theoretically examined this system via analyzing the resonant interaction of a doppler shifted electron beam mode with the modes of the conducting boundary system. The location of these resonant interactions in frequency agrees well with the observed spectrum.

I. Introduction

The interest in high power microwave/millimeter sources in the past few years has resulted from possible applications in such areas as heating of fusion plasmas, particle accelerators, and communications. Among these new sources are gyrotrons, free electron lasers, and relativistic magnetrons. In this paper, we report studies of another such source in which high power radiation is generated at high harmonics of the relativistic electron cyclotron frequency ω_c by the resonant interaction of a fast rotating E-layer beam mode with the waveguide modes of a magnetron-type conducting boundary. This concept was first reported by our group in 1981[1] after extensive work on microwave production in hollow and coaxial boundary systems.[2] Recent theoretical studies[3] indicate that these rotating beam-slotted wall systems should operate over a wide range of electron energies and currents and at frequencies into the millimeter regime. We have also initiated work to explore the low electron energy regime.[4] The potential of such devices to produce radiation near high harmonics of the electron cyclotron frequency makes them especially attractive because of the relatively low applied magnetic field required compared to gyrotrons and magnetrons operating at the same frequency.

In Fig. 1, a schematic of the experimental configuration is shown. A rotating E-layer is produced by passing a hollow nonrotating beam through a narrow symmetric magnetic cusp. The downstream axis encircling particles propagate along various inner and/or outer conducting wall structures. The cross-section of a slotted structure on both the inside and outside walls is shown in Fig. 2. The outer surface of the inner wall has a radius R_i and the outer wall a radius R_o. The beam of radius R_b (~ 6 cm) rotates at a velocity $V_\phi \sim c$ in the region between the inner and outer wall. The depth of the slots is indicated by d_s. We have examined systems in which the number of slots is 12 or 20 placed on either the inner or outer walls or both. We present theoretical (Section II) and experimental (Section III) studies of the production of radiation in these slotted wall systems.

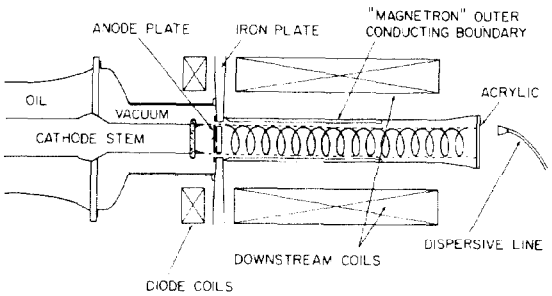

FIG. 1. Schematic of experimental system.

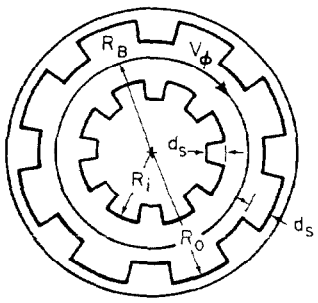

FIG. 2. Cross section of downstream slotted-wall cylindrical tube.

II. Model of Beam-Slotted Waveguide Interaction

The general dispersion relation describing the TE mode structure of a slotted wall conductor as shown in Fig. 2 can be derived by first solving the wave equation for H_z in the slot spaces and the interaction region [$R_i < r < R_o - d_s$, see Fig. 2] separately and then matching the corresponding tangential electric and magnetic fields. The resulting equations can then be solved by expanding the eigenfunctions of both regions in terms of the other and applying Floquet's Theorem for periodic systems. The result can be calculated independently for each mode ℓ' of the slot region. The dispersion relation for a slotted outer wall and no inner wall is

*Work supported by the Air Force Office of Scientific Research and the University of Maryland Computer Science Center.

0018-9499/83/0800-3429$01.00©1983 IEEE

$$D_{\ell\ell'}(k) \equiv \frac{J_{\ell'}(kR_w)N'_{\ell'}(kR_o) - J'_{\ell'}(kR_o)N_{\ell'}(kR_w)}{J'_{\ell'}(kR_w)N'_{\ell'}(kR_o) - J'_{\ell'}(kR_o)N'_{\ell'}(kR_w)}$$

$$- \frac{N_s \Delta\theta}{2\pi} \begin{Bmatrix} 1, & n' = 0 \\ 2, & n' \neq 0 \end{Bmatrix} \times \sum_m \frac{F^2_{\ell\ell'}}{4} \times \frac{J_\ell(kR_w)}{J'_\ell(kR_w)} = 0 \quad (1)$$

where $\ell' = \pi n'/\Delta\theta$, $n' = 0,1,2,\ldots$, $\ell = \ell_o + mN_s$, $k^2 = \omega^2/c^2 - k_z^2$, $R_w = R_o - d_s$, $\Delta\theta$ is the solid angle subtended by one slot, N_s is the number of slots, and ℓ_o represents the phase shift from slot to slot of the field profile. We have defined

$$F_{\ell\ell'} = \frac{\sin\frac{\Delta\theta}{2}(\ell + \ell')}{\frac{\Delta\theta}{2}(\ell + \ell')} + (-1)^{n'} \frac{\sin\frac{\Delta\theta}{2}(\ell - \ell')}{\frac{\Delta\theta}{2}(\ell - \ell')}. \quad (2)$$

This dispersion relation includes not only the TEM slot resonances but the higher order resonances as well. For the case $\ell' = 0$ (constant electric field across the slot gap) the result reduces to that obtained by Collins.[5] As an example, the mode structure ($k_z = 0$) for an outer magnetron wall with 12 (N_s) slots, $\ell' = 0$, $d_s = 1$ cm, and $R_o = 7.5$ cm is shown in Fig. 3. The dots represent the discrete magnetron cutoff frequencies and have the same dependence on k_z as in the hollow waveguide. The numbered connecting lines from dot to dot merely serve to distinguish one radial mode n_r from another. Also shown is the beam mode $\omega = \ell_o\omega_c = \ell_o V_\phi/R_b$ for $\gamma_o = 6$, $R_b = 6$ cm. Note that the mode structure is periodic every $\ell_o = 12$ (N_s) and the relative reduction in phase velocity as compared to hollow waveguide modes.[2]

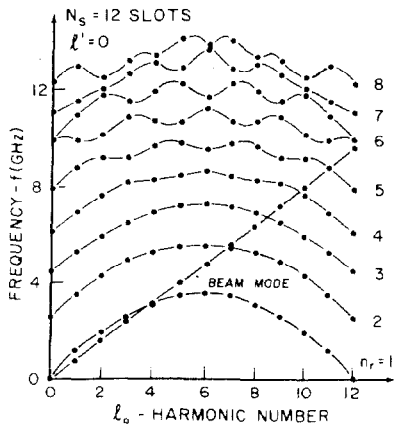

FIG. 3. Discrete mode structure for hollow waveguide with outer magnetron type boundary with parameters R_o = 7.5 cm, d_s = 1 cm, N_s = 12, ℓ' = 0, $\Delta\theta = \pi/N_s$. Beam mode line for γ_o = 6, R_b = 6 cm.

The linear analysis representing the interaction of a beam wave with the modes of the waveguide proceeds by first linearizing the equations of motion and then fourier transforming them to ω-k space. The equation of continuity is then applied to obtain the perturbed charge and current densities. These are then substituted into Maxwell's equations and solved with the magnetron type boundary conditions. From this a modified dispersion relation is obtained defining the interaction of the beam mode with the waveguide mode. The resulting first order modified dispersion relation for the fundamental mode m = 0 is

$$D_{\ell\ell'}(k) = - \frac{N_s \Delta\theta \nu\omega_c^2(\ell^2 - k^2R_b^2)}{\pi\gamma_o kR_w \psi_\ell^2} \times \frac{F^2_{\ell\ell'}}{4} \left[\frac{J'_{\ell_o}(kR_b)}{J'_{\ell_o}(kR_w)}\right]^2 \quad (3)$$

where $\psi_\ell = \omega - \ell_o\omega_c - k_z V_z$, $\nu = e^2 n_s \mu_o R_b/2m_o$ and n_s is the beam surface density. This analysis represents an extension of a planar model studied in Ref. 6.

For the case of resonant interaction, $\psi_\ell \sim 0$ and $D_{\ell\ell'}(k) \sim 0$, one can obtain an explicit expression for the growth rate, $\mathrm{Im}\omega = \omega_I$,

$$\frac{\omega_I}{\omega_c(\frac{\nu}{\gamma_o})^{1/3}} = \frac{\sqrt{3}}{2} \left\{ \frac{N_s \Delta\theta}{\pi\omega_c} \frac{1}{kR_w} \frac{(\ell_o^2 - k^2R_b^2)}{|D'_{\ell\ell'}(k_\ell)|} \times \frac{F^2_{\ell\ell'}}{4} \frac{J'_{\ell_o}(k_\ell R_b)^2}{J'_{\ell_o}(k_\ell R_w)^2} \right\}^{1/3} \quad (4)$$

where

$$D_{\ell\ell'}(k_\ell) = 0, \quad D'_{\ell\ell'}(k_\ell) = \frac{\omega}{kc^2} \left.\frac{\partial D_{\ell\ell'}(k)}{\partial k}\right|_{k=k_\ell}.$$

In Fig. 4, the growth rate as given in Eq. (4) is plotted vs. ℓ_o for the system parameters used in the mode structure shown in Fig. 3. The number associated with each curve represents interaction with the same labeled radial mode as in Fig. 3. Note that resonance in most cases requires a finite k_z. Since the growth rates for the various modes are approximately equal, we surmise that the radial field profile in the interaction space and/or the starting conditions play an important role as to which mode(s) is present. If we examine Eq. (1) and look for modes ($\ell_o = N_s = 12$) that have a substantial field component near the slot, we see that the mode corresonding to $n_r = 6$ (9.8 GHz) or near the zero of $J'_{12}(kR_w)$ has a field profile that peaks near the outer wall. In this case, we would expect good coupling between the waveguide and slot. The other lower radial mode numbers represent zeros near $J'_o(kR_w)$ which has a field profile that is more evenly distributed.

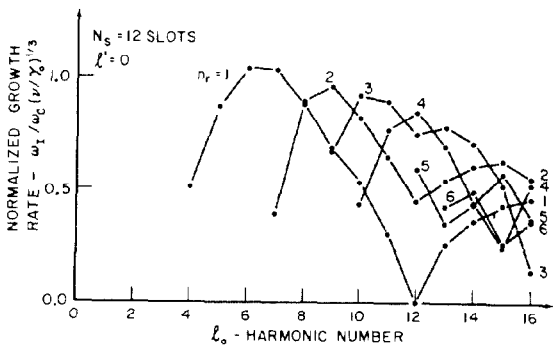

FIG. 4. Normalized growth rate for resonant beam-waveguide interaction including finite k_z. Same parameters as in Fig. 3.

III. Experimental Results

The experimental configuration is shown in Fig. 1. Hollow, nonrotating, relativistic electron beams (2 MeV, 20 kA, 30 ns) are emitted from a circular knife edge carbon cathode. A 0.5 cm wide circular slit aligned with the cathode knife edge allows a fraction of the electron beam to pass through the magnetic cusp transition region where the $v_z \times B_r$ force in this transition region converts most of the axial particle motion into azimuthal motion. The resulting rotating beam propagates in the downstream region with an axial velocity in the range 0.1-0.3 c and interacts with various conducting boundary

configurations. The radiation produced is extracted out the downstream end of the drift chamber as shown in Fig. 1. The downstream end of the drift chamber is flared to allow a smooth transition to free space, and the radiation is picked up by receiving horns connected to X-band (8-12 GHz), Ku band (12-18 GHz), and Ka band (24-40 GHz) dispersive waveguide lines 36 m in length. These dispersive lines are connected to calibrated attenuators and calibrated detectors. The spectrum is determined using standard dispersive line theory and total power is computed by multiplying the power measured at the detector by factors associated with the dialed in attenuation, the frequency dependent attenuation of the dispersive lines, and the ratio of the total area over which radiation is observed to that of the receiving horn.

The results of these experiments are presented in Fig. 5. Figures 5(a) and 5(b) show the measured spectrum for a rotating beam of radius R_b = 6 cm interacting with an empty circular waveguide of radius 7.5 cm. These results show the characteristic broad band spectrum associated with this configuration with power levels of around 200 kW.[2] Figures 5(c) through 5(f) show the resulting spectra obtained by inserting various slotted boundaries into the empty waveguide. Figure 5(c) shows the radiated power spectrum from the interaction of the beam with a slotted outer wall and no inner conductor. The outer conductor radius R_o is 7.5 cm and the slot depth d_s is 1 cm. The applied magnetic field is 1375 G. The number of slots N_s is 12. The large peak observed at 9.6 GHz corresponds to the expected resonant point near $12\omega_c$ (f_c = 770 MHz) and represents an increase in power over the empty waveguide case by a factor of 10^3. Figure 5(d) shows the radiated power spectrum for a rotating beam interacting with a slotted inner conductor and a smooth outer boundary. In this case, N_s = 20, R_o is 7.5 cm, the inner radius R_i is 5.3 cm, and d_s is 0.4 cm. The applied magnetic field is 1387 G. A dominant peak at 16 GHz that corresponds approximately to the $20\ \omega_c$ resonant point is seen with an output of 30 MW. Figure 5(e) shows the results for a different 20 slot case in which the beam radius R_b is reduced to 5.25 cm and R_i is reduced to 4.85 cm, the magnetic field is set at 1575 G. These new conditions shift the cyclotron frequency up to 990 MHz which causes the $20\ \omega_c$ resonance to be pushed up to 20 GHz, although the power fell to about 3 MW. The drop in power by a factor of 10 for the smaller radius case can best be explained by referring to Fig. 6. Figure 6 is a plot of the axial beam current passing through the cusp as a function of the applied magnetic field. The optimum operating range for the R_b = 6 cm beam is at 1350-1415 G with a maximum injected current of about 3 kA. The optimum operating range of the new 5.25 cm radius beam is at a field of 1550-1600 G and a current of about 1 kA. If it is presumed that power is proportional to the square of the beam density and therefore to the square of the beam current, the factor of 2-3 drop in the injected current would cause a reduction in the radiated power by a factor of 4-9.

Figure 5(f) shows the radiated power spectrum for a rotating beam propagating between N_s = 20 slotted inner and outer conductors (180° out of phase). In this case, R_o = 7.5 cm, R_i = 5.0 cm, d_s = 0.64 cm, and R_b = 6 cm. The applied magnetic field is 1400 G. Theoretical analysis of such "glide symmetric" systems[7] indicate that as the two slotted walls are brought closer together, the effective periodicity of the system approaches half of that possessed by either slotted wall alone. As can be seen, the radiated power was largely moved up to 36 GHz, near $40\omega_c$. We are initiating theoretical work on this new concept.

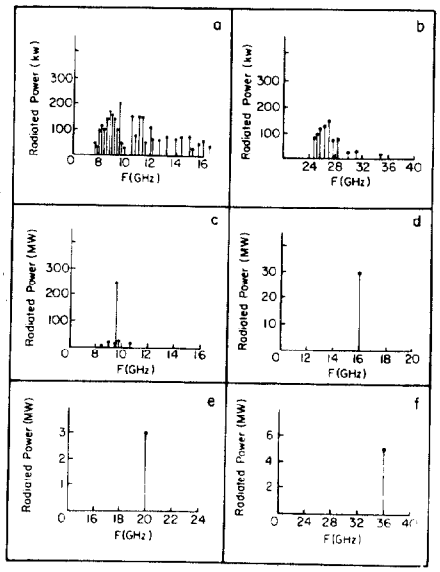

FIG. 5. Typical single shot power spectra. Smooth outer wall, no inner wall: (a) X-band, (b) Ka-band. Slotted wall structures: (c) 12 outer, (d) 20 inner, smooth outer, R_b = 6.0 cm, (e) same as (d) except R_b = 5.25 cm, (f) 20 inner/outer. Geometry is in the text.

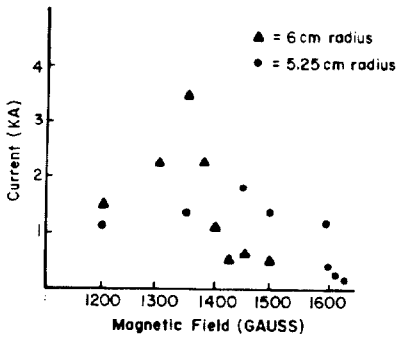

FIG. 6. Axial beam current passing through cusp as a function of magnetic field for R_b = 6.0 cm, R_b = 5.25 cm.

References

1. W. W. Destler, R. L. Weiler, and C. D. Striffler, Appl. Phys. Lett. 38, 570 (1981).
2. W. W. Destler, H. Romero, C. D. Striffler, R. L. Weiler, and W. Namkung, J. Appl. Phys. 52, 2740 (1981).
3. Y. Y. Lau and L. R. Barnett, Int. J. of Infrared and Millimeter Waves, 3, 619 (1982) and Int. J. of Electronics, Oct. 1982.
4. W. Namkung, W. W. Destler, W Lawson, and C. D. Striffler, Bull. Am. Phys. Soc. 27, 1062 (1982).
5. G. B. Collins, "Microwave Magnetrons," p. 56, McGraw Hill, 1948.
6. W. W. Destler, R. Kulkarni, C. D. Striffler, and R. L. Weiler, J. Appl. Phys., (to be published).
7. R. Mittra and S. Lappati, Canadian J. of Phys. 43, 353 (1965).